High-resolution detection of geologic boundaries from potential field anomalies, An enhanced analytic signal technique

Article *in* Geophysics · January 1998

3 authors, including:

Some of the authors of this publication are also working on these related projects:

Project   TAIGER Project View project

Project   TAiwan Integrated Geodynamics Research Project View project

High-resolution detection of geologic boundaries from potential-field anomalies: An enhanced analytic signal technique

Shu-Kun Hsu*, Jean-Claude Sibuet[‡], and Chuen-Tien Shyu**

ABSTRACT

A high-resolution technique is developed to image geologic boundaries such as contacts and faults. The outlines of the geologic boundaries can be determined by tracing the maximum amplitudes of an enhanced analytic signal composed of the nth-order vertical derivative values of two horizontal gradients and one vertical gradient. The locations of the maximum amplitudes are independent of the ambient potential field. This technique is particularly suitable when interference effects are considerable and/or when both induced and remanent magnetizations are not negligible. The corresponding depth to each geologic boundary can be estimated from the amplitude ratio of the enhanced and the simple analytic signals, which provides a simple estimation technique.

Such a method has been applied to magnetic data acquired in the Ilan Plain of Taiwan located at the southwestern end of the Okinawa Trough. The quantitative analysis shows that the underlying geologic boundaries deepen southward and slightly eastward. The enlargement of the Ilan Plain in the direction of the Okinawa Trough and the existence of north-northwest and west-northwest trending faults near the city of Ilan reveal a discontinuity between the Okinawa Trough backarc extension and the compressional process in Taiwan.

INTRODUCTION

Since the early 1970s a variety of automatic or semiautomatic methods, based on the use of the horizontal and/or the vertical gradients (derivatives) of potential-field anomalies, have been developed as efficient tools for the determination of geometric parameters, such as locations of boundaries and depths of the causative sources (e.g., O'Brien, 1971; Nabighian, 1972, 1974; Cordell, 1979; Rao et al., 1981; Thompson, 1982; Murthy, 1985; Barongo, 1985; Blakely and Simpson, 1986; Hansen et al., 1987; Hansen and Simmonds, 1993; Reid et al., 1990; Keating and Pilkington, 1990; Ofoegbu and Mohan, 1990; Roest et al., 1992; Marcotte et al., 1992; Marson and Klingele, 1993). The success of these methods results from the fact that quantitative or semiquantitative solutions are found with no or few assumptions. For instance, the main advantage of using the maximum amplitudes of the analytic signal to determine the location of the structural boundaries is that the result is independent of the earth's magnetic field parameters and of the direction of source magnetization (Nabighian, 1972, 1974; Roest et al., 1992). Such an invariable characteristic is advantageous in magnetic interpretation, especially when the contribution from remanent and induced magnetizations cannot be distinguished.

Thompson (1982) adopted Euler deconvolution to find locations and depths of 2-D geologic boundaries. Later, his approach was successfully applied to 3-D gridded data in Reid et al. (1990). A drawback of using Euler deconvolution is that the user must define the structural index prior to its application. Unfortunately, the choice of structural index is crucial for the determination of the solutions. Cordell (1979) and Cordell and Grauch (1985) used only the maximum amplitudes of the horizontal gradients (without the vertical gradient) to locate near-vertical geologic boundaries from gravity or pseudogravity anomalies. In essence, the horizontal-gradient method is a special case of the use of the analytic signal where the gravity anomaly is equivalent to the vertical magnetization anomaly from the same causative body through Poisson's relationship (Baranov, 1957). In this case, even if we do not add the vertical gradient in computing the amplitude of the analytic signal, in the absence of interference, the resulting amplitude (a bell-

shaped function) also has its maximum value directly over the abrupt boundaries [cf. equation (2) Nabighian, 1972].

Since potential-field data correspond to the superposition of effects from all causative sources, the determination of geologic boundaries usually suffers from nearby source interference that yields mislocations (Grauch and Cordell, 1987). To reduce interference effects, one may downward continue the data. Although this technique may provide increased resolution, it is not very stable with respect to taking high-order derivatives (Nabighian, 1974). Following the suggestion of Nabighian (1974) for the 2-D case, in the present paper, we propose an enhanced analytic signal technique for the interpretation of 3-D potential field anomalies.

THEORY

For 2-D and 3-D potential-field anomalies, Nabighian (1972, 1984) has demonstrated that the horizontal and the vertical gradients form a pair of Hilbert transforms or analytic signals. One important characteristic is that the amplitude of the analytic signal, composed of these orthogonal gradients, exhibits a bell-shaped symmetric function located directly above the boundary of the structure (e.g., contact or fault). This idea had been explained extensively in Nabighian (1972, 1974) in the 2-D case and used in 3-D magnetic interpretation by Roest et al. (1992). Because of interference effects, the use of the simple analytic signal in the 3-D case seems insufficient to detect geologic boundaries (see discussion in Mohan, 1993). Since the existing interference is usually inevitable, improving resolution becomes a requirement.

In the 2-D case, Nabighian (1974) suggested using the following bell-shaped function to enhance the analytic signal from shallow sources:

$$\left(\frac{\partial^n G_h}{\partial h^n}\right)^2 + \left(\frac{\partial^n G_z}{\partial h^n}\right)^2 = \frac{(1^2 \times 2^2 \times 3^2 \times \cdots \times n^2)\alpha^2}{(d^2 + h^2)^{n+1}}, \tag{1}$$

where G_h and G_z are the horizontal and vertical gradients of the potential-field anomaly, respectively; h is the distance along the horizontal axis which is perpendicular to the strike of the 2-D structure; n is a positive integer; d is the depth to the top surface of the source, while the lower surface is at infinity; α is the ambient parameter and is equal to $2kFc \sin \theta$ when the step model of magnetic anomaly is applied; k is the susceptibility contrast of the step model; F is the earth's magnetic field magnitude; θ is the dip angle of the step model; $c = 1 - \cos^2 i \sin^2 B$ for total magnetic field anomalies; i is the inclination of the earth's magnetic field; and B is the angle between magnetic north and positive h - axis.

In the 3-D case, the simple analytic signal is defined in Nabighian (1984) as

$$A_0(x, y) = \frac{\partial G}{\partial x}\hat{x} + \frac{\partial G}{\partial y}\hat{y} + i\frac{\partial G}{\partial z}\hat{z}, \tag{2}$$

and its amplitude as

$$|A_0(x, y)| = \sqrt{(G_x)^2 + (G_y)^2 + (G_z)^2}, \tag{3}$$

where G is the potential-field anomaly,

$$G_x = \frac{\partial G}{\partial x}; \; G_y = \frac{\partial G}{\partial y},$$

and

$$G_z = \frac{\partial G}{\partial z}.$$

To extend equation (1) into the 3-D case, we define the nth-order enhanced analytic signal as

$$A_n(x, y) = \frac{\partial}{\partial x}\left(\frac{\partial^n G}{\partial z^n}\right)\hat{x} + \frac{\partial}{\partial y}\left(\frac{\partial^n G}{\partial z^n}\right)\hat{y} + i\frac{\partial}{\partial z}\left(\frac{\partial^n G}{\partial z^n}\right)\hat{z}, \tag{4}$$

and its amplitude as

$$|A_n(x, y)| = \sqrt{(\nabla^n G_x)^2 + (\nabla^n G_y)^2 + (\nabla^n G_z)^2}, \tag{5}$$

where $\nabla^n = \partial^n/\partial z^n$.

For $n = 2$, equation (4) corresponds to the enhanced analytic signal derived from second vertical derivative, and the amplitude of equation (5) becomes

$$|A_2(x, y)| = \sqrt{(\nabla^2 G_x)^2 + (\nabla^2 G_y)^2 + (\nabla^2 G_z)^2}. \tag{6}$$

Equation (6) is used hereafter as an example to demonstrate the improvement of the detection of geologic boundaries. First of all, it is noted that the amplitude of enhanced and simple analytic signals are invariant with respect to the coordinate system (see the Appendix). Considering that the observed surface is outside the sources, Laplace's equation is satisfied for the potential-field anomalies (Grant and West, 1976, 213) then

$$\frac{\partial^2}{\partial x^2} + \frac{\partial^2}{\partial y^2} + \frac{\partial^2}{\partial z^2} = 0. \tag{7}$$

Considering equations (1) and (7) in the absence of interference effects from nearby boundaries (ideal situation), for one geologic boundary of an arbitrary strike, equation (1) can be written in the 3-D case (see the derivation in detail in the Appendix) as

$$\left(\frac{\partial^n G_x}{\partial z^n}\right)^2 + \left(\frac{\partial^n G_y}{\partial z^n}\right)^2 + \left(\frac{\partial^n G_z}{\partial z^n}\right)^2$$
$$= \frac{(1^2 \times 2^2 \times 3^2 \times \cdots \times n^2)\alpha^2}{(d^2 + h^2)^{n+1}}. \tag{8}$$

Hence, each maximum amplitude of the second-order enhanced analytic signal (at $h = 0$), being a peak of a bell-shaped function, is written as

$$|A_2(x, y)|_{\max} = \frac{|2\alpha|}{d^3}, \tag{9}$$

while the corresponding maximum amplitude of the simple analytic signal in the 3-D case is (cf. the 2-D case in Nabighian, 1974):

$$|A_0(x, y)|_{\max} = \frac{|\alpha|}{d}. \tag{10}$$

Equations (8) (9) and (10) suggest at least two possible ways of estimating the depth to the top of the boundary. One is to estimate the offset from the position of the maximum amplitude to a specific position where the amplitude is, for example, $|A_2(x, y)|_{\max}/2\sqrt{2}$ (i.e., when $h = d$); however, this is

not easily done in practice. The other is to compute the depth from the amplitude ratio of equations (9) and (10); i.e.,

$$d = \sqrt{2} \times \sqrt{\frac{|A_0(x, y)|_{max}}{|A_2(x, y)|_{max}}}. \qquad (11)$$

For real data, in addition to interfering anomalies, several factors may induce bias in the locations of the geologic boundaries and the estimation of the corresponding depths. For instance, the assumption of an infinite bottom surface is unrealistic. Thus, we should assume either that the geologic boundaries are near-vertical (abrupt) or that step-like sources are thick enough to give sufficient resolution for discriminating the locations of the top and the bottom boundaries. The larger the distance between the top and bottom surfaces, the better the resolution is obtained to detect individual boundaries or edges. Because of the enhancement of the analytic signal, the detection resolution for location (or outline) of geologic boundaries is increased and the result is less affected by interference. Equation (11) is used for estimating the depths to boundaries, even though it is not completely valid because of the fact that the locations of maxima for the enhanced and the simple analytic signals may be different on account of interference effects. For depth estimation, we use the amplitude of the simple analytic signal at the location defined by the maximum amplitude of the second-order enhanced analytic signal. This may lead to some depth discrepancies depending on the extent of interference effects. However, peak values of amplitudes are less influenced from interference effects than their nearby values and such a depth estimation approach will be shown to be efficiently simple. Alternatively, the depth estimation from the amplitude ratio concept could be achieved by introducing another maximum amplitude such as the maximum amplitude of the first-order enhanced analytic signal (see the Appendix). Once the depth for each location of the maximum amplitude of the enhanced analytic signal has been obtained, the ambient parameter a can be estimated, for example, from equation (9).

Since numerical approximation for the gradient and the curvature values (by finite-difference method and/or Fourier transform) is required, we should pay close attention to the occurrence of high-frequency error and ensure that the observed data are smooth enough to avoid unwanted effects.

The maximum amplitudes of both the enhanced and the simple analytic signals are not independent of α, the ambient parameter of equations (9) and (10). They are related to the intensity of the magnetization (kF), the inclination (i) of the earth's field, and the strike (B) of the geologic boundary. For a given geologic boundary, the amplitude of the enhanced analytic signal becomes small when the geologic boundary is close to the magnetic equator or when its strike is near parallel to the magnetic north [i.e., c in equation (1) becomes close to zero]. For this reason, caution is needed for the boundary identification directly over the amplitude image of analytic signals derived from magnetic anomalies. By contrast, for gravity anomalies, the amplitudes of analytic signals are independent of latitudes and boundary orientations and are related only to density contrasts and depths of boundaries.

The locations of the maximum amplitudes of the enhanced analytic signal can be automatically determined by the method in Blakely and Simpson (1986) or can be defined from maps of the amplitudes.

TEST CASES

Isolated source (model 1)

For simplicity, the magnetic anomaly shown in Figure la, was produced by using a 5×5 km^2 infinite rectangular vertical prism (Bhattacharyya, 1964) located at a depth of 3 km (Figure 1f, parameters in Table 1). Results of the simple simple analytic signal method used in Roest et al. (1992) (Figure 1) and of the method we propose (Figure 2) are compared. Horizontal gradients of Figure la along the x and y directions (Figures 1b and 1c) are calculated on a 0.2 km grid spacing with a 5-point finite-difference method derived from the method of undetermined coefficients (Gerald and Wheatley, 1984, A5). The vertical gradient deduced from Figure la (Figure 1d) is calculated by the generalized Hilbert transform (Nabighian, 1984). Figure le shows the amplitude of the analytic signal (Roest et al., 1992) deduced from the three components of Figures 1b, 1c, and 1d. Because of the interference effects, none of the boundaries are detected. By using the method of Blakely and Simpson (1986) with indices 2 and 3, only three maxima are found (Figure 1f).

To obtain the enhanced amplitude of the second-order enhanced analytic signal [equation (6)], we use the same grid spacing and the 5-point, finite-difference method as above. The curvature values of Figures 1b, 1c, and 1d are approximated to produce the three required components (Figures 2b, 2c, and 2d). Because the numerical computation is an approximation, high-frequency noise appears in the background. However, when the amplitudes of the enhanced analytic signal are computed, the background noise significantly decreases (Figure 2e) and generally a threshold control of enhanced amplitudes can be assigned to improve the degree of confidence. As shown in Figures 2e and 2f, the maximum amplitudes of the enhanced analytic signal delineate the boundaries of the prism quite well. The locations of maxima, determined by the method of Blakely and Simpson (1986) using indices 2 and 3 and amplitudes greater than 5 nT/km^3 (threshold control) to avoid numerical approximation errors, show that this method achieves a higher resolution than the simple analytic signal method (cf. Figures 1f and 2f). Depths to the top surface are estimated between 2.03 to 2.25 km from equation (11) instead of 3 km in the given model. This provides about 70% accuracy in depth estimation; however, we shall mention again that the performance of depth estimation depends on the extent of the interference effects if the amplitude ratio method is applied.

Multiple sources (model 2)

To demonstrate that the ambient magnetic parameters do not influence detection of geologic boundaries, a more sophisticated model is adopted (Figure 3). The characteristics of each prism are shown in Table 1. The same procedure used for model 1 was repeated to get the amplitudes of the enhanced and simple analytic signals. Figure 4a displays the amplitudes of the simple analytic signal used by Roest et al. (1992). Clearly, the maximum amplitudes used to determine the boundaries exhibit much interference, especially for the boundaries of prism 2C which is shallower than prism 2B and has a smaller intensity of magnetization than prism 2A. This interference phenomenon is also revealed in Figure 5a, where
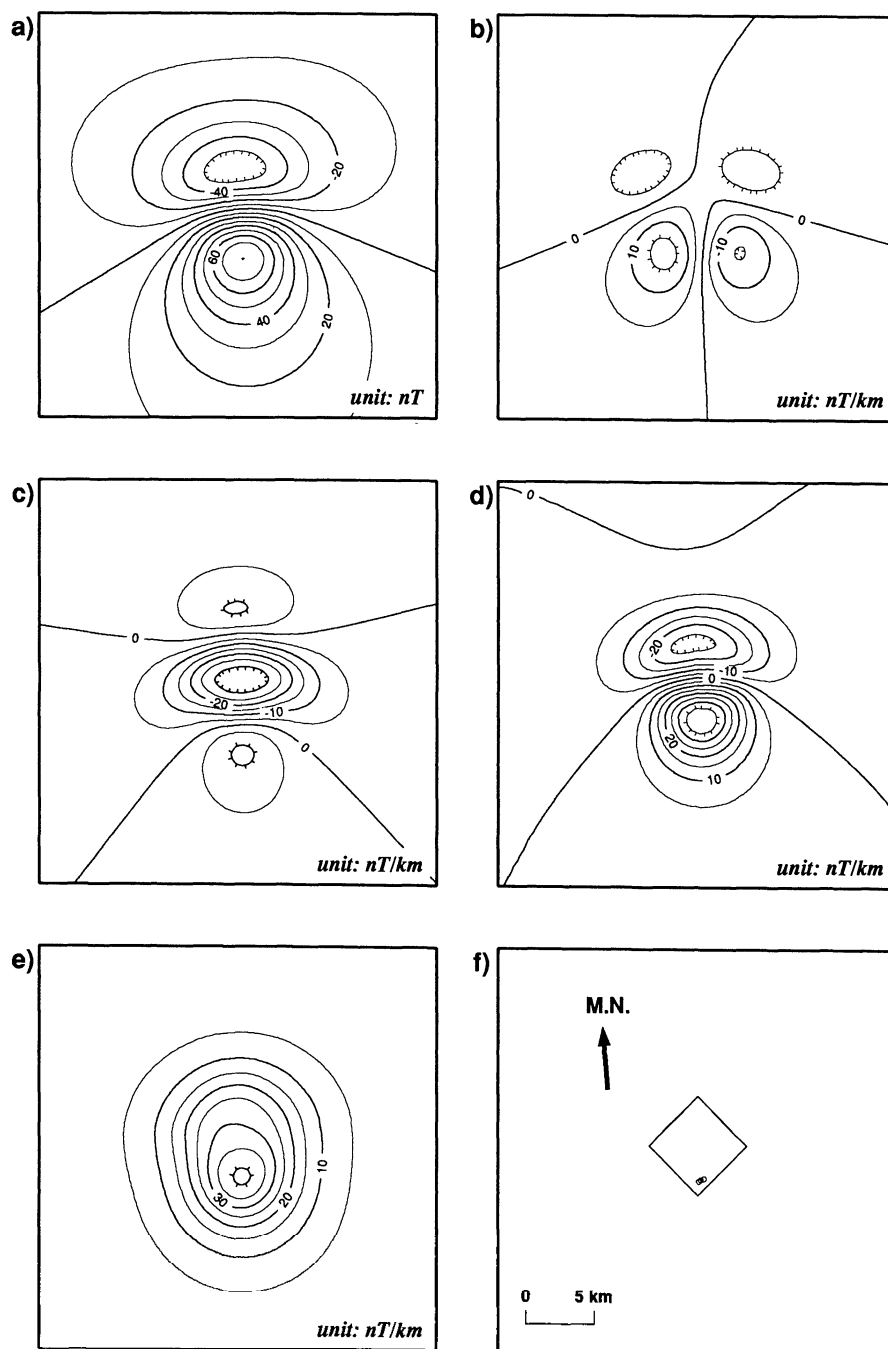
FIG. 1. (a) Total-field magnetic anomaly of model 1 (Table 1). (b) Horizontal - x gradient of (a). (c) Horizontal - y gradient of (a). (d) Vertical gradient of (a). (e) Amplitudes of the analytic signal from (b), (c) , and (d). (f) Locations of maxima of (e) (open circles), determined by the method of Blakely and Simpson (1986). Solid lines represent the boundary of model 1. Solid arrows indicate the declination of the magnetization. M.N.: magnetic north.

Table 1. Magnetic parameters for the rectangular vertical prisms of the test models. D.E.: declination of the earth's field. I.E.: inclination of the earth's field. D.M.: declination of the magnetization. I.M.: inclination of the magnetization. h1: depth to the top surface. h2: depth to the bottom surface. I.O.M.: intensity of the magnetization (nT).

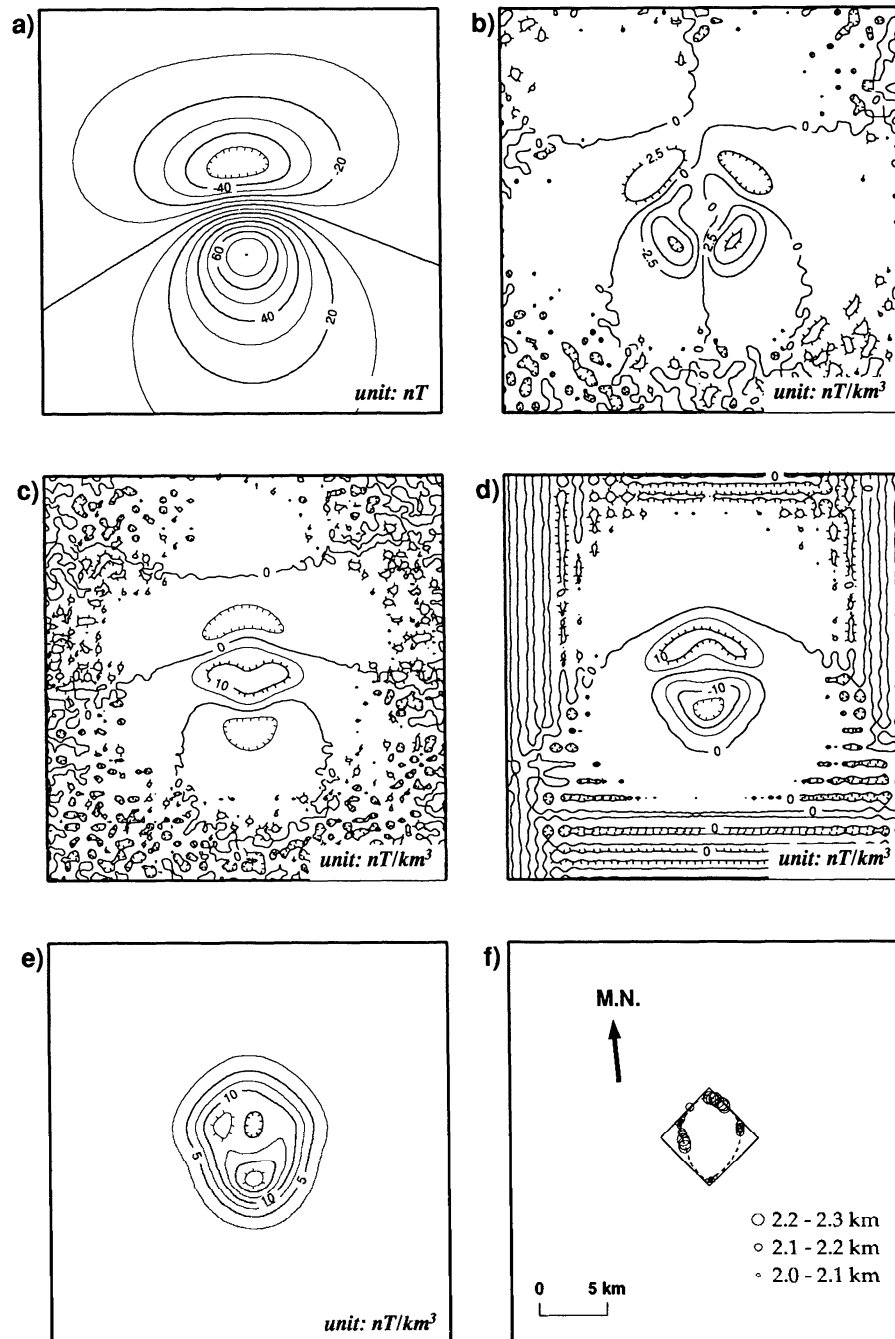|		D.E.	I.E.	D.M.	I.M.	length	width	h1	h2	I.O.M.
model 1		- 5 °	35°	- 5 °	35°	5 km	5 k m	3 k m	infinite	100
model 2	2 A	-1 0 °	40°	0°	35°	10 km	5 k m	2 k m	10 km	100
	2B	-1 0 °	40°	-10°	40°	10 km	5 k m	1 k m	10 km	60
	2C	-1 0 °	40°	170°	20°	10 km	5 k m	2 k m	10 km	80

FIG. 2. Enhanced analytic signal of model 1 (Table 1). (a) Total-field magnetic anomaly of model 1. (b) Curvature values of the horizontal-x gradient. (c) Curvature values of the horizontal-y gradient. (d) Curvature values of the vertical gradient. (e) Amplitudes calculated from (a), (b), and (c). (f) Locations of maxima of (e) (open circles), determined by the method of Blakely and Simpson (1986). The corresponding depths are estimated from equation (11). Solid arrows indicate the declination of the magnetization. M.N.: magnetic north. Solid line is the boundary of the model 1. Dotted line is the outline of the maximum amplitudes traced by hand.
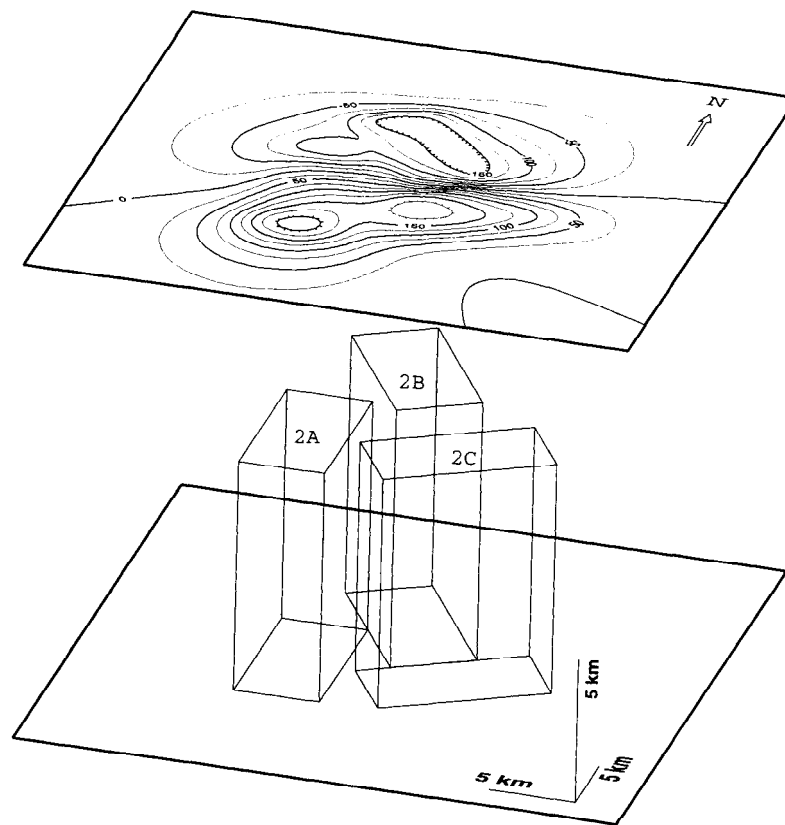
FIG. 3. Schematic outlines of model 2 and corresponding total-field magnetic anomaly. Magnetic parameters for each vertical rectangular prism are indicated in Table 1. Contour interval is 25 nT.
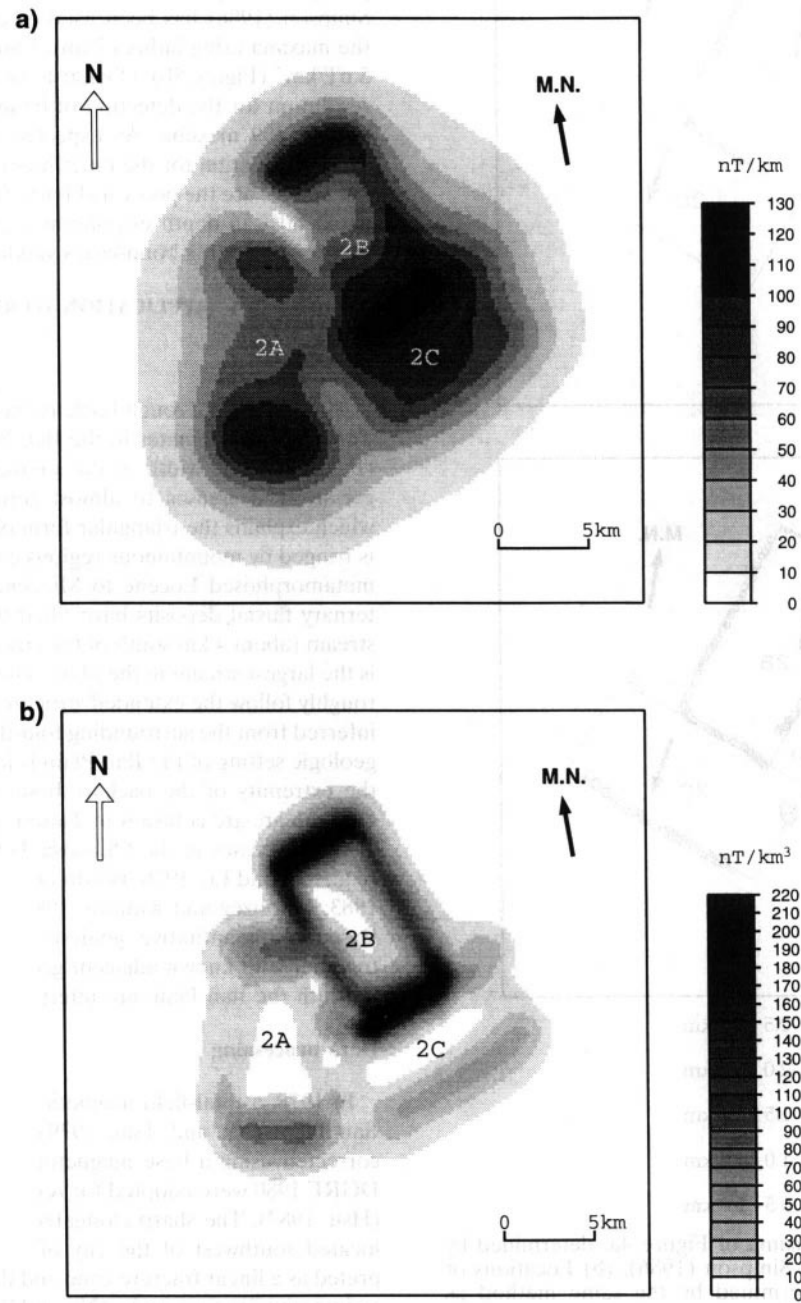
FIG. 4. (a) Amplitudes of the analytic signal of model 2 obtained by the method of Roest et al. (1992). (b) Amplitudes of the second-order enhanced analytic signal (this study). Solid arrows indicate the declination of the magnetization. M.N.: magnetic north. Note that the boundaries whose strikes are more perpendicular to the declination of the magnetization present large amplitudes and that the amplitude decreases when the top surface is deeper.
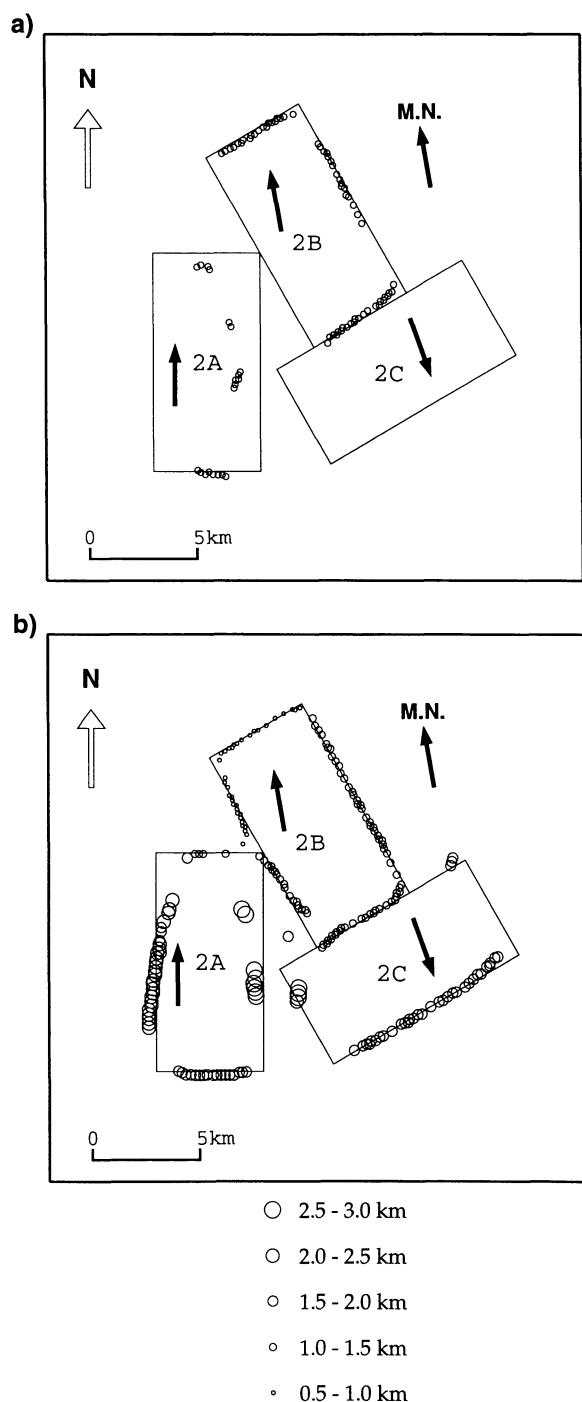
FIG. 5. (a) Locations of maxima of Figure 4a, determined by the method of Blakely and Simpson (1986). (b) Locations of maxima of Figure 4b, determined by the same method as above. Corresponding depths are estimated from equation (11). Solid arrows indicate the declination of the earth's field and the declination of the magnetization of each prism. M.N.: magnetic north. Solid lines are the boundaries of model 2 shown in Figure 3.

none of maxima for the prism 2C is detected except for the contiguous boundary between prisms 2C and 2B. By contrast, the enhanced analytic signal (Figure 4b) clearly identifies the boundaries of prisms. Note that the large amplitudes are

associated with the shallow prism (2B) and that the effect of the boundary orientations with respect to the magnetic north (e.g., east-west trending boundaries of prism 2A) is clearly identified in Figure 4b. Similarly, the amplitudes are very weak for the right and left boundaries of prism 2C, which are almost parallel to magnetic north. The same method of Blakely and Simpson (1986) has been used to determine the locations of the maxima using indices 2 and 3 and amplitudes greater than 5 nT/km^3 (Figure 5b). Obviously, our method exhibits a higher resolution for the detection of boundaries with the identification of 209 maxima. As expected from interference effects, depth estimation for the inner boundaries between prisms 2A, 2B, and 2C are the poorest (Figure 5b). An average accuracy of about 80% in depth estimation is given in this case with the east-west trending boundaries yielding better depth estimates.

APPLICATION TO REAL DATA

Ilan Plain

The Okinawa Trough backarc basin extends from Japan to Taiwan and terminates in the Ilan Plain, northeastern Taiwan (Figure 6). The width of the southern Okinawa Trough progressively decreases to almost zero west of the Ilan Plain, which explains the triangular form of the Ilan Plain. The plain is fringed by mountainous regions composed mainly of slightly metamorphosed Eocene to Miocene rocks (Figure 7). Quarternary fluvial deposits have filled the plain. The Lanyanghsi stream (about 4 km south of the city of Ilan), flowing eastward, is the largest stream in the plain. The stream and its tributaries roughly follow the extended structural lineations, which can be inferred from the surrounding fold-thrust belts (Figure 7). The geologic setting of the Ilan Plain is important in the sense that the extremity of the backarc basin was narrowed associated with the arc-arc collision in Taiwan (Hsu et al., 1995). Extensional processes in the Okinawa Trough have been discussed (e.g., Lee and Lu, 1976; Bowin et al., 1978; Eguchi and Uyeda, 1983; Letouzey and Kimura, 1985; Sibuet et al., 1987, 1995). Based on quantitative analysis of the magnetic anomalies together with known adjacent geology, the geologic structures beneath the Ilan Plain are interpreted.

Data processing

In 1978, a total-field magnetic survey was conducted in the Ilan Plain (Yu and Tsai, 1979). The diurnal variation was corrected using a base magnetometer. The DGRF 1975 and DGRF 1980 were adopted for removal of the secular variation (Hsu, 1987). The sharp elongated negative magnetic anomaly located southwest of the city of Ilan (Figure 8a) was interpreted as a linear fracture zone and the positive linear anomaly as intrusive igneous rocks (Yu and Tsai, 1979). If the latter is assumed to be produced by a 2-D thick dike, the depth to the top surface of the intrusive body was estimated at 1.5-2.0 km and the width of the dike 4.7-5.7 km on the eastern side of the plain (Yu and Tsai, 1979; Hsu, 1987).

Following the same procedure used for the test cases, the distribution of amplitudes of the second-order enhanced analytic signal was obtained on a regular 0.2 km grid spacing (Figure 8b). The detected locations of maxima as well as the estimated depths are shown in Figure 8c. The unknown geology beneath the Ilan Plain is inferred (Figure 9) by using

Figures 7 and 8c. The sedimentological facies beneath the plain are inferred from the surrounding geology (e.g., Ho, 1986) and are subject to further modification. The linear structure located in the lower part of the surveyed area (Figure 8c) is suspected to be an artifact caused by bad data reduction in a mountainous region.

New geologic insight

On the basis of Figures 8c and 9, new geologic insight is proposed for the Ilan Plain. Several geologic boundaries located southwest of Ilan are east-west trending and tend to deepen southward and slightly eastward (Figure 8c). This reflects the existence of the southern flank of the underlying anticline whose axis is along facies 8 (Figure 9). The two well-defined northern boundaries are interpreted as the eastern prolongations of the two contacts between the Eocene and Oligocene sedimentary units (facies 7 and 8 in Figure 9). They are buried less than 1 km beneath the fluvial deposits and abruptly terminate at the west side of the city of Ilan. The east-west trending boundary (1.5-2.5 km beneath the plain), located 6 km south of Ilan, is probably the prolongation of the Lishan Fault, a major tectonic feature that has been interpreted as the boundary fault between the Hsiiehshan Range (the belt between faults I and II in Figures 7 and 9) on the west and the Miocene Lushan Formation (facies 3 in Figures 7 and 9). The Lishan Fault is considered to be a major thrust that dips steeply to the east (Biq, 1971; Wu, 1978); however, its northern part is not clear (Wu, 1978; Ho, 1986). This fault is still active and its seismicity suggests that its northeastern extension has a normal motion consistent with the extension system of the Okinawa Trough backarc basin (Tsai et al., 1975). Since the prolongation of the Lishan Fault into the Ilan Plain is not well imaged (Figure 8c), the continuation of the Lishan Fault into the Ilan Plain may be complex or it may not

be a simple fault. However, a recent study suggests that the Lishan Fault corresponds to a suture zone along the axis of an ancient backarc basin uplifted because of the arc-arc collision in Taiwan (Hsu et al., 1995; Hsu and Sibuet, 1995). All the roughly east-west features, including the Lishan Fault, stop abruptly or change orientations near the city of Ilan. This suggests the existence of a major north-northeast left lateral strike-slip fault located just beneath Ilan. East of this fault, the geologic boundaries, about 1.5-2 km deep, present an eastward fan-shaped geometry that could be associated with the backarc extension of the Okinawa Trough.

In summary, our proposed geologic picture below the Quaternary deposits of the Ilan Plain (Figure 9) indicates a discontinuity between the tensional (to the east) and compressional (to the west) features in terms of strike-slip faults near the city of Ilan. The river system of the Ilan Plain is more or less controlled by the geologic boundaries as revealed by the similarity of the river system and the geologic boundaries (cf. Figures 7 and 9).

CONCLUSIONS

Based on vertical derivatives, the concept of using the 3-D enhanced analytic signal has been developed to reduce the effect of interference between closely spaced anomalies. This technique has the advantage of avoiding dependence on the ambient magnetic field and of aiding quantitative interpretation of potential-field anomalies. The improved resolution allows us to better detect geologic boundaries of causative sources. The determination of depths to the top surfaces of causative boundaries from amplitude ratios of analytic signals [e.g., equation (11)] is feasible under several assumptions: the different resolution of the two analytic signals used to compute the depths must be accepted; each individual source must be considered as homogeneous; and the signal from the bottom
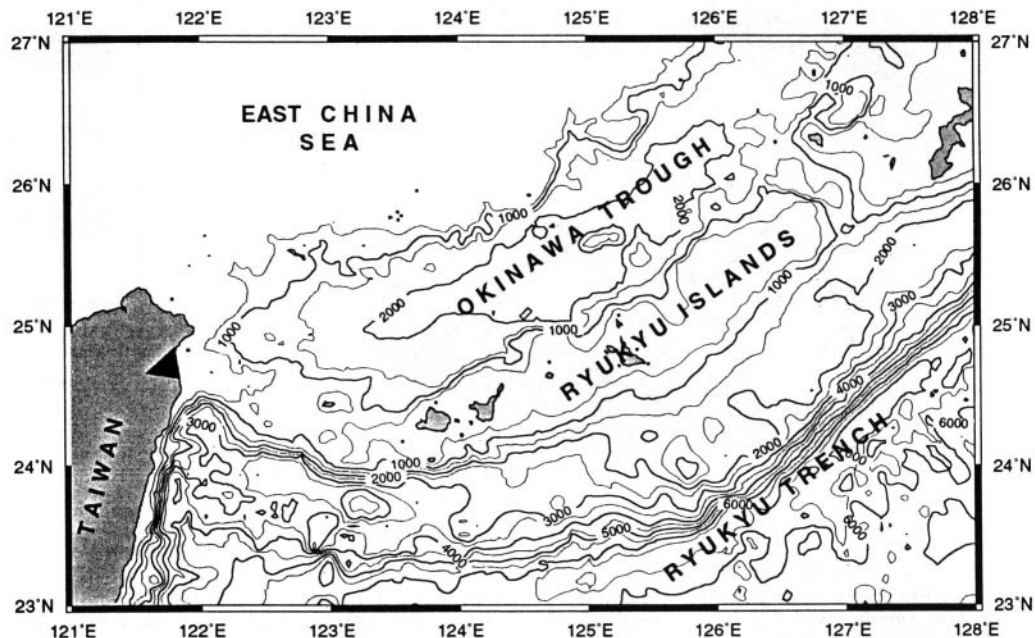

FIG. 6. The Ilan Plain (black area in northern Taiwan) is located at the southwestern tip of the Okinawa Trough.

surface of the source must be negligible. Care is needed for interpretation of amplitudes of the analytic signals derived from magnetic anomalies. Even though the locations of the maxima are directly over the geologic boundaries, the amplitudes vary as a function of α, the ambient magnetic field parameter.

The improvement in resolution from the proposed technique provides a better visualization of outlines of geologic features. Such information could be used as a constraint when applying inversion or forward techniques. In addition, the quantitative analysis of the locations of geologic boundaries and associated depths is well suited to the method of Blakely and Simpson (1986).

This method has been applied to magnetic data acquired in the Ilan Plain (northeastern Taiwan). The deduced tectonic and sedimentological map below the Quaternary deposits of the Ilan Plain shows that the collisional process in Taiwan and the extensional backarc formation of the Okinawa Trough are disconnected by the occurrence of strike-slip faults near the city of Ilan.
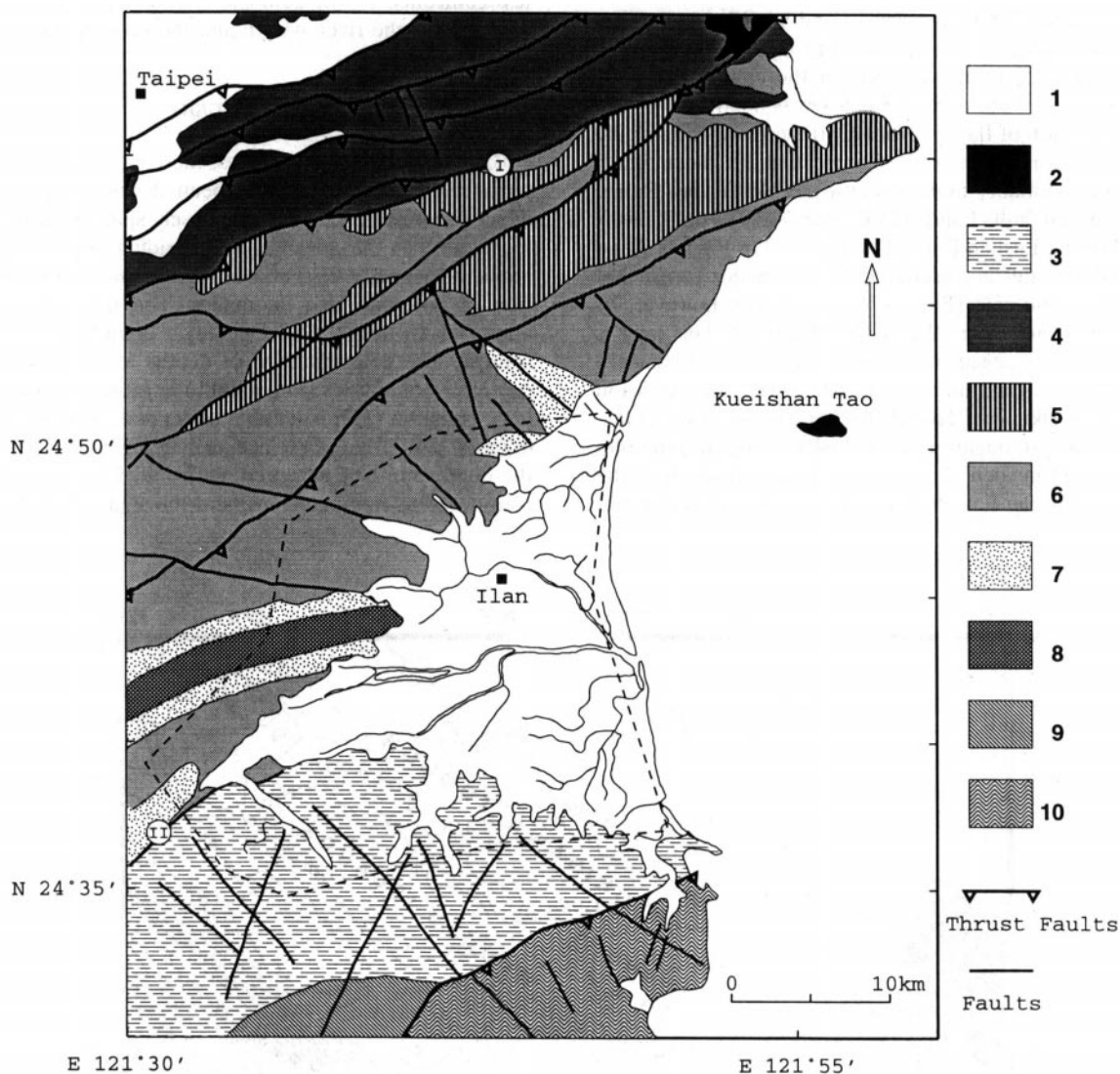
ACKNOWLEDGMENTS

FIG. 7. Geologic map around the Ilan Plain (after Ho, 1986) with the major faults detected from satellite data (after Tsai, 1986). 1 = Recent clay, sand and gravel. 2 = Pleistocene andesite and andesitic pyroclastics. 3 = Miocene argillite, slate, phyllite and sandstone interbeds. 4 = Early and Middle Miocene sandstone and shale. 5 = Oligocene to Miocene sandstone, shale and coaly shale. 6 = Oligocene argillite, slate and indurated sandstone. 7 = Oligocene quartzitic sandstone, slate and graphitic shale. 8 = Eocene to Oligocene slate, phyllite with sandstone interbeds. 9 = Eocene slate, phyllite with quartzitic sandstone interbeds. 10 = Late Paleozoic and Mesozoic shist and gneiss. I = Chuchih fault. II = Lishan fault. The very thin lines represent streams in the Ilan Plain. The dashed line is the limit of the magnetic survey.
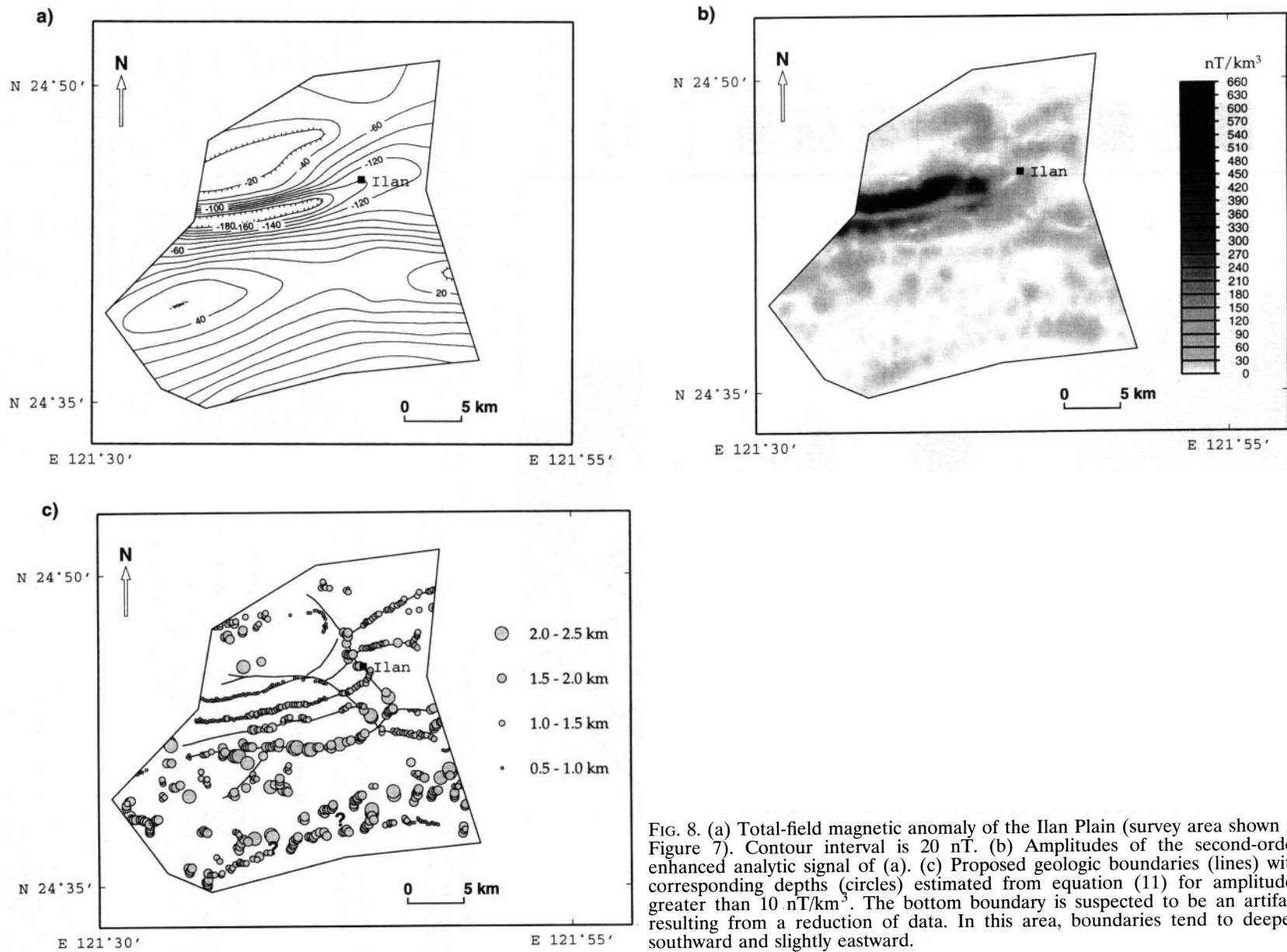
FIG. 8. (a) Total-field magnetic anomaly of the Ilan Plain (survey area shown in Figure 7). Contour interval is 20 nT. (b) Amplitudes of the second-order enhanced analytic signal of (a). (c) Proposed geologic boundaries (lines) with corresponding depths (circles) estimated from equation (11) for amplitudes greater than 10 nT/km^3. The bottom boundary is suspected to be an artifact resulting from a reduction of data. In this area, boundaries tend to deepen southward and slightly eastward.
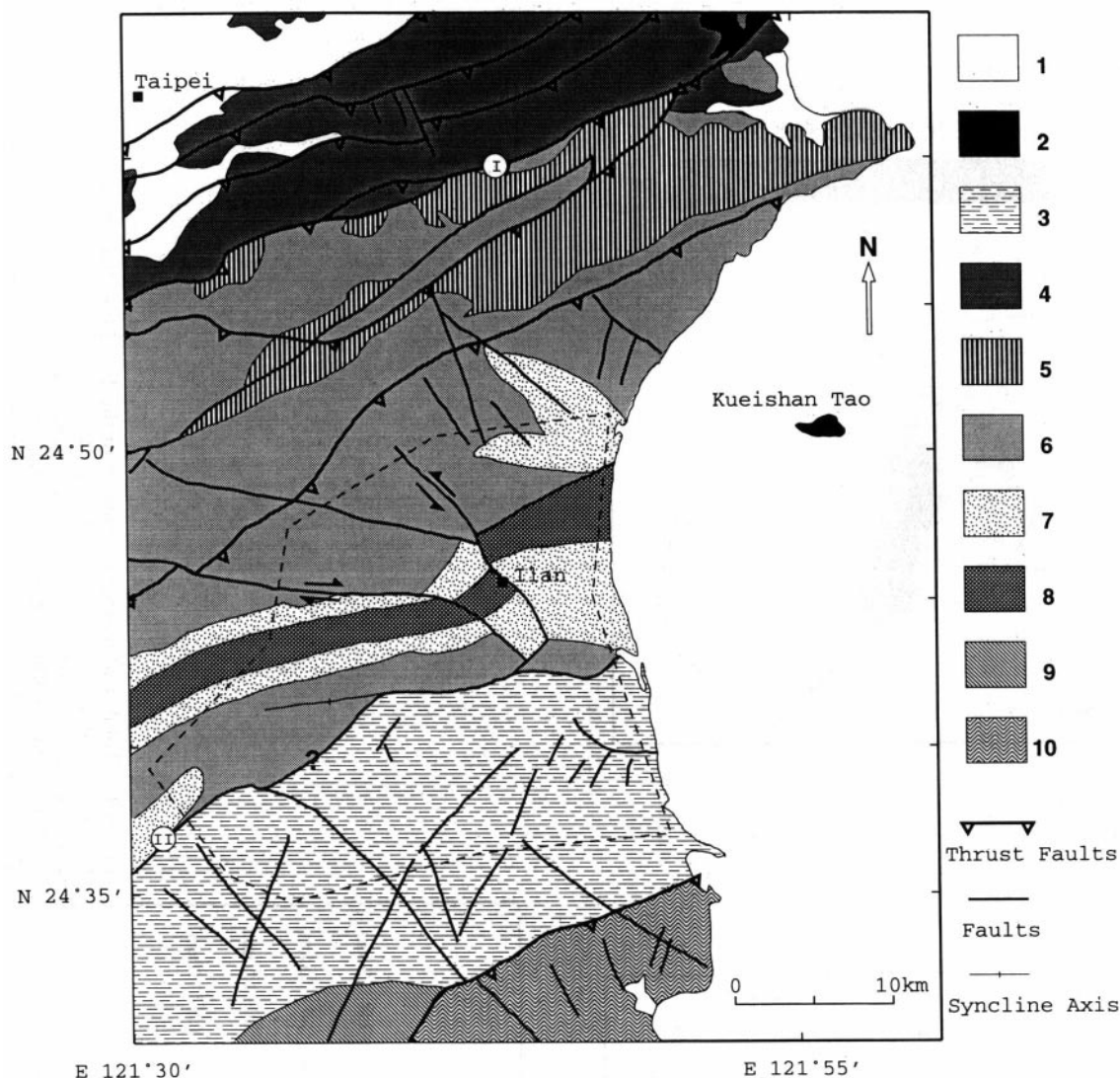
FIG. 9. Interpreted geologic map of the Ilan Plain area. Geologic context beneath the Ilan Piain is completed by adding the information of Figure: 8c and by inferring the sedimentological facies from the surrounding geology of Figure 7. The dashed line is the limit of the magnetic survey. Same legend as for Figure 7.

REFERENCES

Baranov, V., 1957, A new method for interpretation of aeromagnetic maps: Pseudogravimetric anomalies: Geophysics, **22,** 359-383.

Barongo, J. O., 1985, Method for depth estimation on aeromagnetic vertical gradient anomalies: Geophysics, **50,** 963-968.

Bhattacharyya, B. K., 1964, Magnetic anomalies due to prism-shaped bodies with arbitrary polarization: Geophysics, **29,** 517-531.

Biq, C.-C., 1971, Some aspects of post-erogenic block tectonics in Taiwan. Recent crustal movements: R. Soc. New Zealand Bull., **9,** 19-24.

Blakely, R. J., and Simpson, R. W., 1986, Approximating edges of source bodies from magnetic or gravity anomalies: Geophysics, **51,** 1494-1498.

Bowin, C., Lu, R. S., Lee, C. S., and Schouten, H., 1978, Plate convergence and accretion in Taiwan-Luzon region: Bull. Am. Assoc. Geol., **62,** 1645-1672.

Cordell, L., 1979, Gravimettic expression of graben faulting in Santa Fe country and the Espanola Basin, New Mexico: New Mexico Geol. Soc. Guidebook, 30th Field Conf., 59-64.

Cordell, L., and Grauch, V. J. S., 1985, Mapping basement magneti-zation zones from aeromagnetic data in the San Juan Basin, New Mexico, *in* Hinze, W. J., Ed., The utility of regional gravity and magnetic anomaly maps: Soc. Explor. Geophys., 181-197.

Eguchi, T., and Uyeda, S., 1983, Seismotectonics of the Okinawa Trough and Ryukyu Arc: Mem. Geol. Soc. China, **5,** 189-210.

Gerald, C. F., and Wheatley, P. O., 1984, Applied numerical analysis, 3rd ed.: Addison-Wesley Pub. Co. Inc.

Grant, F. S., and West, G. F., 1976, Interpretation theory in applied geophysics: McGraw-Hill Inc.

Grauch, V. J. S., and Cordell, L., 1987, Limitations of determining density or magnetic boundaries from the horizontal gradient of gravity or pseudogravity data: Geophysics, **52,** 118-124.

Hansen, R. O., Pawlowski, R. S., and Wang, X., 1987, Joint use of analytic signal and amplitude of horizontal gradient maxima for three-dimensional gravity data interpretation: 57th Ann. Internat. Mtg., Soc. Expl. Geophys., Expanded Abstracts, 100-102.

Hansen, R. O., and Simmonds, M., 1993, Multiple-source Wenner deconvolution: Geophysics, **58,** 1792-1800.

Ho, C.-S., 1986, An introduction to the geology of Taiwan: Explantory text of the geologic map of Taiwan: The ministry of economic affairs, Rep. of China, 2nd ed.

Hsu, S.-K., 1987, Using DGRF models and approximated derivatives

to reduce datum-level error and to interpret magnetic anomalies: MS. thesis, National Taiwan University (in Chinese).

Hsu, S.-K., and Sibuet, J.-C., 1995, Is Taiwan the result of arc-continent or arc-arc collision?: Earth Planet. Sci Lett., **136,** 315-324.

Hsu, S.-K., Sibuet, J.-C., and Monti, S., 1995, Arc-arc collision vs. backarc extension: Taiwan mountain building: International conference and 3rd Sino-French symposium on the active collision in Taiwan, Program and extended abstracts: Geol. Soc. China, Taiwan, Rep. of China, 121-130.

Keating, P. B., and Pilkington, M., 1990, An automated method for the interpretation of magnetic vertical-gradient anomalies: Geophysics, **55,** 336-343.

Lee, C.-S., and Lu, R. S., 1976, Significance of the southwestern section of Ryukyu Inner Ridge in the exploration of geothermal resources in Ilan area: Mining Technical Digest, **14,** 114-120. (in Chinese).

Letouzey, J., and Kimura, M., 1985, Okinawa trough genesis: Structures and evolution of a backarc basin developed in a continent: Marine and Petr. Geol., **2,** 111-130.

Marcotte, D. L., Hardwick, C. D., and Nelson, J. B., 1992, Automated interpretation of horizontal magnetic gradient profile data: Geophysics, **57,** 288 -295.

Marson, I., and Klingele, E. E., 1993, Advantages of using the vertical gradient of gravity for 3-D interpretation: Geophysics, **58,** 1588-1595.

Mohan, N. L., 1993, Discussion on "Magnetic interpretation using the 3-D analytic signal (by Roest, W. R., Verhoef, J., and Pilkington, M., 1992: Geophysics, **57,** 116-125): Geophysics, **58,** 1214.

Murthy, I. V. R., 1985, Magnetic interpretation of dike anomalies using derivatives: PAGEOPH, **123,** 232-238.

Nabighian, M. N., 1972, The analytic signal of two-dimensional magnetic bodies with polygonal cross-section: Its properties and use for automated anomaly interpretation: Geophysics, **37,** 507-517.

——— 1974, Additional comments on the analytic signal of two-dimensional magnetic bodies with polygonal cross-section: Geophysics, **39,** 85-92.

——— 1984, Toward a three-dimensional automatic interpretation of potential field data via generalized Hilbert transforms: Fundamental relation: Geophysics, **49,** 957-966.

O'Brien, D. P., 1971, CompuDepth: A new method for depth to basement computation: Presented at the 42th Ann. Internat. Mtg., Soc. Expl. Geophys.

Ofoegbu, C. O., and Mohan, N. L., 1990, Interpretation of aeromagnetic anomalies over part of southeastern Nigeria using three-dimensional Hilbert transformation: PAGEOPH., **134,** 13-29.

Rao, D. A., Babu, H. V., and Narayan, P. V., 1981, Interpretation of magnetic anomalies due to dikes: The complex gradient method: Geophysics, **46,** 1572-1578.

Reid, A. B., Allsop, J. M., Granser, H., Millett, A. J., and Somerton, I. W., 1990, Magnetic interpretation in three dimensions using Euler deconvolution: Geophysics, **55,** 80 -91.

Roest, W. R., Verhoef, J., and Pilkington, M., 1992, Magnetic interpretation using the 3-D analytic signal: Geophysics, **57,** 116-125.

Sibuet, J.-C., Hsu, S.-K., Shyu, C.-T., and Liu, C.-S., 1995, Structural and kinematic evolutions of the Okinawa Trough backarc basin, in Taylor, B., Ed., Backarc basins: Tectonics and magmatism, Plenum, 343-379.

Sibuet, J.-C., Letouzey, J., Barbier, F., Char-vet, J., Foucher, J.-P., Hilde, T. W. C., Kimura, M., Chiao, L.-Y., Marsset, B., Muller, C., and Stéphan, J.-F., 1987, Backarc extension in the Okinawa Trough: J. Geophys. Res., **92,** 14 041-14 063.

Thompson, D. T., 1982, EULDPH: A new technique for making computer-assisted depth estimates from magnetic data: Geophysics, **47,** 31-37.

Tsai, Y.-B., 1986, Seismotectonics of Taiwan: Tectonophysics, **125,** 17-38.

Tsai, Y.-B., Feng, C. C., Chiu, J. M., and Liaw, H. B., 1975, Correlation between microearthquakes and geologic faults in the Hsintien-Ilan area: Petr. Geol. Taiwan, **12,** 149-167.

Wu, F. T., 1978, Recent tectonics of Taiwan: J. Phys. Earth, **26,** suppl., 265-299.

Yu, S.-B., and Tsai, Y.-B., 1979, Geomagnetic anomalies of Ilan Plain: Taiwan: Petr. Geol. Taiwan, **16,** 19-27.

Wessel, P., and Smith, W. H. F., 1991, Free software helps map and display data: EOS, trans. Am. Geophys. Union, **72,** 441-446.

APPENDIX A-RELATIONSHIPS BETWEEN ENHANCED AMPLITUDES AND BOUNDARY DEPTHS

Any pair of orthogonal horizontal gradients in a Cartesian coordinate system, for example G_x and G_y, can be rotated to a new coordinate system. If a system is rotated an arbitrary angle Φ counter-clockwise, then the new horizontal gradients can be expressed as

$$G_{x'} = G_x \cos(\Phi) - G_y \sin(\Phi), \qquad (A-1)$$

$$G_{y'} = G_x \sin(\Phi) + G_y \cos(\Phi). \qquad (A-2)$$

Taking the gradient operator $\nabla^n = \partial^n/\partial z^n \ (= \partial^n/\partial z'^n)$ and defining $\nabla^0 = 1$, equations (A-l) and (A-2) become

$$\nabla^n G_{x'} = \nabla^n(G_x \cos(\Phi) - G_y \sin(\Phi))$$
$$= \cos(\Phi)\nabla^n G_x - \sin(\Phi)\nabla^n G_y, \qquad (A-3)$$

and

$$\nabla^n G_{y'} = \nabla^n(G_x \sin(\Phi) + G_y \cos(\Phi))$$
$$= \sin(\Phi)\nabla^n G_x + \cos(\Phi)\nabla^n G_y. \qquad (A-4)$$

By combining the square values of each side of equations (A-3) and (A-4), we obtain

$$(\nabla^n G_{x'})^2 + (\nabla^n G_{y'})^2 = (\nabla^n G_x)^2 + (\nabla^n G_y)^2. \qquad (A-5)$$

Since the vertical component $G_{z'} = G_z$ everywhere, then $\nabla^n G_{z'} = \nabla^n G_z$, and

$$(\nabla^n G_{x'})^2 + (\nabla^n G_{y'})^2 + (\nabla^n G_{z'})^2 = (\nabla^n G_x)^2 + (\nabla^n G_y)^2 + (\nabla^n G_z)^2. \ (A-6)$$

Equation (A-6) demonstrates that the amplitudes of both the enhanced ($n \geq 1$) and the simple ($n = 0$) analytic signals are invariant with respect to the coordinate system. Furthermore, if the y'-direction is chosen to be parallel to the strike of a given geologic boundary (i.e., $G_{y'} = 0$ and $\partial^n/\partial y'^n = 0$) and Laplace's equation is valid (i.e., $\partial^2/\partial z'^2 = -\partial^2/\partial x'^2$ because $\partial^2/\partial y'^2 = 0$), the square value of the amplitude of the nth-order enhanced analytic signal [i.e., equation (A-6)] becomes

$$(\nabla^n G_x)^2 + (\nabla^n G_y)^2 + (\nabla^n G_z)^2 = (\nabla^n G_{x'})^2 + (\nabla^n G_{z'})^2$$

$$= \left(\frac{\partial^n}{\partial z'^n}\frac{\partial G}{\partial x'}\right)^2 + \left(\frac{\partial^n}{\partial z'^n}\frac{\partial G}{\partial z'}\right)^2,$$

$$= \left(\frac{\partial^n}{\partial x'^n} G_{x'}\right)^2 + \left(\frac{\partial^n}{\partial x'^n} G_{z'}\right)^2, \text{ if } n = 2m;$$

$$\text{or} = \left(\frac{\partial^n}{\partial z'^{(2m-1)}} G_{x'}\right)^2 + \left(\frac{\partial^n}{\partial z'^{(2m-1)}} G_{z'}\right)^2$$

$$= \left(\frac{\partial^{2(m-1)}}{\partial z'^{2(m-1)}}\frac{\partial}{\partial z'}\frac{\partial}{\partial x'} G\right)^2 + \left(\frac{\partial^{2(m-1)}}{\partial z'^{2(m-1)}}\frac{\partial}{\partial z'}\frac{\partial}{\partial z'} G\right)^2$$

$$= \left(\frac{\partial^{2(m-1)}}{\partial x'^{2(m-1)}}\frac{\partial}{\partial z'}\frac{\partial}{\partial x'} G\right)^2 + \left(\frac{\partial^{2(m-1)}}{\partial x'^{2(m-1)}}\frac{\partial}{\partial x'^2} G\right)^2$$

$$= \left(\frac{\partial^n}{\partial x'^n} G_{z'}\right)^2 + \left(\frac{\partial^n}{\partial x'^n} G_{x'}\right)^2, \text{ if } n = 2m - 1,$$

$$(A-7)$$

where m is a positive integer.

In the absence of interference effects, equation (A-7) of the 3-D case is essentially equivalent to equation (1) of the 2-D case. Accordingly, a general form of equation (1) for one geologic boundary, can be written in the 3-D case as

$$\left(\frac{\partial^n G_x}{\partial z^n}\right)^2 + \left(\frac{\partial^n G_y}{\partial z^n}\right)^2 + \left(\frac{\partial^n G_z}{\partial z^n}\right)^2$$

$$= \frac{(1^2 \times 2^2 \times 3^2 \times \cdots \times n^2)\alpha^2}{(d^2 + h^2)^{n+1}}. \quad (A\text{-}8)$$

Each maximum amplitude of the nth-order enhanced analytic signal (at $h = 0$) is therefore related to a depth d of an arbitrary trending boundary by writing

$$|A_n(x, y)|_{max} = \sqrt{(\nabla^n G_x)^2 + (\nabla^n G_y)^2 + (\nabla^n G_z)^2}\Big|_{max}$$

$$= \frac{|1 \times 2 \times 3 \times \cdots \times n \times \alpha|}{d^{n+1}}. \quad (A\text{-}9)$$

For example, each maximum amplitude of the first-order enhanced analytic signal ($n = 1$), used by Marson and Klingele (1993) corresponds to

$$|A_1(x, y)|_{max} = \sqrt{(\nabla^1 G_x)^2 + (\nabla^1 G_y)^2 + (\nabla^1 G_z)^2}\Big|_{max}$$

$$= \frac{|\alpha|}{d^2}. \quad (A\text{-}10)$$

For $n = 2$, the relationship in equation (9) is used in this study. High-order enhanced analytic signal can substantially reduce interference effects, whereas, in real data the noise is also relatively amplified, which may render interpretation questionable except that potential data are quite smooth. In addition, 3-D enhanced amplitudes of more than second-order are not easily achievable.